

# Effective macroscopic transport parameters between parallel plates with constant concentration boundaries

D.R. Webster <sup>\*</sup>, D.S. Felton, J. Luo

*School of Civil and Environmental Engineering, Georgia Institute of Technology, Atlanta, GA 30332-0355, USA*

Received 7 November 2006; received in revised form 1 April 2007; accepted 9 April 2007

Available online 29 April 2007

## Abstract

A macroscopic transport model is developed, following the Taylor shear dispersion analysis procedure, for a 2D laminar shear flow between parallel plates possessing a constant specified concentration. This idealized geometry models flow with contaminant dissolution at pore-scale in a contaminant source zone and flow in a rock fracture with dissolving walls. We upscale a macroscopic transient transport model with effective transport coefficients of mean velocity, macroscopic dispersion, and first-order mass transfer rate. To validate the macroscopic model the mean concentration, covariance, and wall concentration gradient are compared to the results of numerical simulations of the advection–diffusion equation and the Graetz solution. Results indicate that in the presence of local-scale variations and constant concentration boundaries, the upscaled mean velocity and macrodispersion coefficient differ from those of the Taylor–Aris dispersion, and the mass transfer flux described by the first-order mass transfer model is larger than the diffusive mass flux from the constant wall. In addition, the upscaled first-order mass transfer coefficient in the macroscopic model depends only on the plate gap and diffusion coefficient. Therefore, the upscaled first-order mass transfer coefficient is independent of the mean velocity and travel distance, leading to a constant pore-scale Sherwood number of 12. By contrast, the effective Sherwood number determined by the diffusive mass flux is a function of the Peclet number for small Peclet number, and approaches a constant of 10.3 for large Peclet number.

© 2007 Elsevier Ltd. All rights reserved.

*Keywords:* Macroscopic model; Taylor–Aris dispersion; Upscaling; Mass transfer; Graetz solution

## 1. Introduction

Understanding the transport characteristics in the subsurface provides a foundation for assessing and remediating sites with source zone contaminants. At these sites, non-aqueous, sorbed, and dissolved phase contaminants stored in stagnant zones act as a long-term reservoir of persistent loading of contaminants to groundwater passing through them [12]. Thus, quantifying the mass flux emanating from the stagnant zones to the relative mobile water zones has been considered as one of the primary tasks for characterizing a contaminant source zone and assessing technology options and decision making.

In the past decade, both experimental and numerical effort has been expended to develop mass transfer correlations for varying hydrodynamic and biochemical conditions to quantify the mass transfer characteristics in contaminant source zone, particularly in the source zone contaminated by non-aqueous phase liquids (NAPLs) e.g., [7,9,17,23,28,32]. Such correlations generally describe macroscopic behavior, which is the collective outcome over an ensemble of pores. The purpose of developing such correlations is to identify the key factors that may control the mass flux released from the contaminant source, and to incorporate the factors in a macroscopic transport model to simulate field-scale remediation processes, predict treatment effects, and help design optimal strategies. However, the critical scale-up issues from pore-scale to larger-scale are often treated as afterthoughts because the developers of the remediation technology typically work at the

<sup>\*</sup> Corresponding author. Tel.: +1 404 894 6704; fax: +1 404 385 1131.  
E-mail address: [dwebster@ce.gatech.edu](mailto:dwebster@ce.gatech.edu) (D.R. Webster).

bench-scale, where local variations are neglected and mixing is assured e.g., [14,29]. Upscaling pore-scale information to macroscopic models in contaminant source zones is not yet well studied.

In the present study, we focus on an idealized flow geometry of hydrodynamically fully developed flow between parallel plates with constant wall concentration, which mimics the contaminant zone where the mass is trapped and feeds the system by diffusion. We upscale the macroscopic transport model with effective transport parameters including effective mean velocity, macroscopic dispersion coefficient, and upscaled first-order mass transfer coefficient from the local-scale variations, which are described exclusively by local transverse coordinates over the plate gap. The approach is similar to the framework of the well-known Taylor–Aris dispersion analysis [3,35], which has been widely used to study macrodispersion behavior, see [6]. The idealized flow geometry is applicable to mimic pore-scale NAPL dissolution [30], to illustrate the segregation effects during reactive transport [18], and to describe transport in a single fracture with contaminants stored in the rock matrix [4]. For instance, fractures in native rock present a difficult technical challenge to waste disposal because dissolved contaminants can leach into a fracture, diffuse into the surrounding walls, and affect the physical and chemical properties of the fracture media [27]. These contaminants can become trapped in the rock matrix, which makes remediation very difficult. Conversely, as water flows through a fracture, the walls can dissolve, i.e. transfer minerals, solutes, or radionuclides from the fracture walls into the aqueous phase. These dissolved solutes can subsequently contaminate local ground water. Furthermore, dissolved minerals can precipitate, coating the fracture walls, which affects sorption of contaminants onto the walls. Other applications include the transport in fracture networks [16], waste management [15], and heat exchangers [19].

This paper is organized as follows. In Section 2 we describe the model development, present the upscaling procedures, and derive the effective macroscopic model. In Section 3, we compare the analytically derived results to numerical simulations and discuss the performance of the upscaled macroscopic model. The conclusion of our findings and recommendations are given in Section 4.

## 2. Model development

### 2.1. Governing equation

Taylor [35] and Aris [3] were the first to analyze the macrodispersion coefficient in a 2D laminar shear flow between parallel plates. In the current work, the inflow has zero concentration and the solute concentration at the wall boundaries is specified as a constant (see Fig. 1). Thus, this geometry represents dissolution of a solute from the walls into clean fluid or contaminant release from a constant source at the walls. The current arrangement differs from

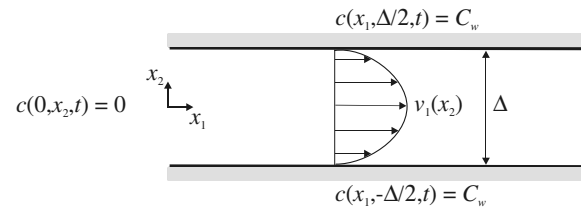


Fig. 1. Definition sketch.

that of Taylor [35], which consisted of contaminated fluid displacing clean fluid in a tube with zero flux at the walls.

For flow between parallel plates the transport equation can be written as

$$\frac{\partial c}{\partial t} + v_1(x_2) \frac{\partial c}{\partial x_1} - d \left( \frac{\partial^2 c}{\partial x_1^2} + \frac{\partial^2 c}{\partial x_2^2} \right) = 0 \quad (1)$$

where  $c$  is the concentration of a solute or another passive scalar quantity,  $d$  is the molecular diffusion coefficient, and  $v_1$  is the velocity in the longitudinal direction,  $x_1$ . The fully developed velocity profile between parallel plates is

$$v_1(x_2) = V_1 \left( \frac{3}{2} - 6 \frac{x_2^2}{\Delta^2} \right) \quad (2)$$

where  $V_1$  is the mean velocity,  $\Delta$  is the gap between the parallel plates, and  $x_2$  is the coordinate in the traverse direction.

The boundary conditions are constant concentration,  $C_w$ , at the parallel walls,

$$c(x_1, \Delta/2, t) = C_w, \quad c(x_1, -\Delta/2, t) = C_w, \quad 0 < x_1 < \infty$$

zero concentration at the inlet,

$$c(0, x_2, t) = 0, \quad -\Delta/2 < x_2 < \Delta/2$$

and zero longitudinal gradient downstream:

$$\frac{\partial c}{\partial x_1}(\infty, x_2, t) = 0, \quad -\Delta/2 < x_2 < \Delta/2$$

For NAPL dissolution problems,  $C_w$  is equal to the saturation concentration in the aqueous phase at the interface between the NAPL and water. The initial condition is zero concentration everywhere in the domain:

$$c(x_1, x_2, 0) = 0, \quad 0 < x_1 < \infty, \quad -\Delta/2 < x_2 < \Delta/2$$

A similar model setup has been used at different scales to study NAPL dissolution. For example, Sahloul et al. [30] approximated the pore-scale flow around a single NAPL ganglion, in which the transverse velocity variation was considered. Further, Chu et al. [9] upscaled a lumped mass transfer coefficient for a bench-scale biologically enhanced NAPL dissolution, in which a macroscopic uniform velocity field was assumed. And, Lee and Chrysikopoulos [22] field-scaled NAPL pool dissolution in stratified and anisotropic porous formations, in which velocity variations at both longitudinal and transverse directions were included.

### 2.2. Graetz solution

The Graetz solution describes the steady state temperature field and heat transfer to flowing fluid between parallel

plates, the same geometry as our model domain. The Peclet number,  $Pe = 2V_1\Delta/d$ , describes the relative importance of transport mechanisms acting on the solute, specifically the ratio of advection relative to molecular diffusion. For high  $Pe$ , longitudinal diffusion can be neglected compared to advection (and transverse diffusion) in the transport equation (Kays and Crawford [19] report that  $Pe$  must be greater than 100). The resulting non-dimensional steady state transport equation follows from Eq. (1) and can be written as

$$\frac{2}{3}v_1^+ \frac{\partial}{\partial x_1'} \left( \frac{C_w - c(x_1', x_2')}{C_w - C_i} \right) = \frac{\partial^2}{\partial x_2'^2} \left( \frac{C_w - c(x_1', x_2')}{C_w - C_i} \right) \quad (3)$$

where  $v_1^+ = v_1/V_1$  is the non-dimensional velocity in the  $x_1$  direction,  $C_i$  is the concentration of the injected solution, and the non-dimensional coordinates are defined as  $x_1' = \frac{16}{3} \frac{1}{Pe} \frac{x_1}{\Delta}$  and  $x_2' = 2 \frac{x_2}{\Delta}$ .

This equation can be solved analytically, by use of separation of variables, for hydrodynamically developed flow between parallel plates with constant wall concentration e.g., [26,33,34]. Inserting the separated functional form into the governing equations yields separate differential equations with respect to  $x_1'$  and  $x_2'$ . The solution with respect to  $x_1'$  is an exponential function. The ordinary differential equation with respect to  $x_2'$  has variable coefficients and can be solved following the method of Frobenius [38]. The solution takes the form of an infinite series. Combining the functional forms yields the solution:

$$\frac{C_w - c(x_1', x_2')}{C_w - C_i} = \sum K_n \exp(-\lambda_n^2 x_1') \times \left( 1 - \frac{\lambda_n^2}{2} x_2'^2 + \frac{\lambda_n^2}{12} \left( \frac{\lambda_n^2}{2} + 1 \right) x_2'^4 + \dots \right) \quad (4)$$

The coefficients,  $K_n = \frac{-2}{\lambda_n^2} \frac{1}{(dx_2/d\lambda_n)_{x_2=1}}$ , are found using Sturm–Liouville theory and the first eight are shown in Table 1 along with the first eight eigenvalues,  $\lambda_n$ . Note that for larger values of  $n$ , convergence of the eigenvalue calculation requires a large number of terms in the series (roughly 100 terms for the eighth eigenvalue shown here). Shah and London [34], among others, also provide asymptotic equations for the eigenvalues.

Integrating the concentration field defined by Eq. (4) across the aperture yields the mean concentration:

Table 1  
Eigenvalues and coefficients for the Graetz solution

$n$	$\lambda_n$	$K_n$	$Z_n$
0	1.6816	1.2005	0.6194
1	5.6699	-0.2991	-0.3208
2	9.6683	0.1608	0.2420
3	13.6677	-0.1074	-0.2019
4	17.6674	0.0796	0.1768
5	21.6672	-0.0628	-0.1591
6	25.6671	0.0512	0.1458
7	29.6670	-0.0483	-0.1353

$$\frac{C_w - C(x_1')}{C_w - C_i} = \frac{1}{2} \int_{-1}^1 \frac{C_w - c(x_1', x_2')}{C_w - C_i} dx_2' = \sum K_n \exp(-\lambda_n^2 x_1') Z_n \quad (5)$$

where  $C$  is the average concentration over the transverse direction,  $x_2$ , and the values of  $Z_n$  are also shown in Table 1.

Agrawal [1], Deavours [10], and Weigand [36], among others, attempted to extend the Graetz solution by incorporating the effects of longitudinal diffusion. In each case, the boundary conditions were modified slightly to facilitate the solution procedure, which prevents direct comparison to the macroscopic transport model presented here.

### 2.3. Upscaling to 1-D macroscopic transport model

The objective of upscaling is to develop a 1-D macroscopic transport model to describe the mean concentration by avoiding the evaluation of local-scale variations. The governing equation can be written as

$$\frac{\partial C}{\partial t} + V_1^* \frac{\partial C}{\partial x_1} - D^* \frac{\partial^2 C}{\partial x_1^2} = K^*(C_w - C) \quad (6)$$

where  $V_1^*$  is the effective mean velocity,  $D^*$  is the macroscopic dispersion coefficient, and  $K^*$  is the upscaled first-order mass transfer coefficient.

By applying the small-perturbation method, the velocity and concentration are decomposed into the cross-sectional mean and deviation:

$$v_1 = V_1 + v_1' \quad \text{and} \quad c = C + c' \quad (7)$$

where the cross-sectional mean is defined by

$$V_1 = \frac{1}{\Delta} \int_{-A/2}^{A/2} v_1(x_2) dx_2 \quad \text{and} \quad C(x_1) = \frac{1}{\Delta} \int_{-A/2}^{A/2} c(x_1, x_2) dx_2 \quad (8)$$

Substituting the decomposition into the 2D transport equation, Eq. (1), gives:

$$\frac{\partial C}{\partial t} + \frac{\partial c'}{\partial t} + V_1 \frac{\partial C}{\partial x_1} + V_1 \frac{\partial c'}{\partial x_1} + v_1' \frac{\partial C}{\partial x_1} + v_1' \frac{\partial c'}{\partial x_1} - d \left( \frac{\partial^2 C}{\partial x_1^2} + \frac{\partial^2 c'}{\partial x_1^2} + \frac{\partial^2 c'}{\partial x_2^2} \right) = 0 \quad (9)$$

Averaging each term of Eq. (9) across the aperture, realizing that the mean of the deviation is zero by definition, and applying the product rule and continuity equation to equate  $v_1' \frac{\partial c'}{\partial x_1}$  to  $\frac{\partial}{\partial x_1} (\overline{c'v_1'})$  yields:

$$\frac{\partial C}{\partial t} + V_1 \frac{\partial C}{\partial x_1} + \frac{\partial}{\partial x_1} (\overline{c'v_1'}) - d \frac{\partial^2 C}{\partial x_1^2} = \frac{d}{\Delta} \left( \frac{\partial c'}{\partial x_2} \Big|_{-A/2}^{A/2} \right) \quad (10)$$

The term  $\frac{\partial}{\partial x_1} (\overline{c'v_1'})$  is the gradient of the covariance between velocity and concentration and physically corresponds to the transport of solute due to the velocity variation across

the aperture. The objective of this analysis is to produce a Fickian model for this term and the wall concentration gradient term on the right hand side of Eq. (10). Hence, the model development described below follows on the method employed by Taylor [35] that involves simplifying Eq. 10 in order to form a model of the unknown terms, specifically  $\frac{\partial}{\partial x_1}(\overline{c'v'_1})$  and  $\left(\frac{\partial c'}{\partial x_2}\right)_{-A/2}$ . The modeled expressions for these terms will be substituted into the full version of Eq. (10) in order to form the 1-D macroscopic transport equation, Eq. (6).

Subtracting Eq. (10) from Eq. (9), and then linearizing (i.e. assuming that the product of two perturbation variables is much smaller than the other terms):

$$\frac{\partial c'}{\partial t} + V_1 \frac{\partial c'}{\partial x_1} - d \left( \frac{\partial^2 c'}{\partial x_1^2} + \frac{\partial^2 c'}{\partial x_2^2} \right) = -v'_1 \frac{\partial C}{\partial x_1} - \frac{d}{A} \left( \frac{\partial c'}{\partial x_2} \right)_{-A/2} \quad (11)$$

Assuming longitudinal diffusion is much smaller than transverse diffusion yields:

$$\frac{\partial c'}{\partial t} + V_1 \frac{\partial c'}{\partial x_1} - d \frac{\partial^2 c'}{\partial x_2^2} = -v'_1 \frac{\partial C}{\partial x_1} - \frac{d}{A} \left( \frac{\partial c'}{\partial x_2} \right)_{-A/2} \quad (12)$$

For small  $Pe$ , the  $V_1 \frac{\partial c'}{\partial x_1}$  term is small compared to the other terms and hence can be neglected, which is consistent with Taylor's analysis [13]. For larger  $Pe$ , the term is expected to be negligible far from the inlet where  $\partial c'/\partial x_1 \approx 0$ . Neglecting this term and assuming steady state yields:

$$-d \frac{\partial^2 c'}{\partial x_2^2} = -v'_1 \frac{\partial C}{\partial x_1} - \frac{d}{A} \left( \frac{\partial c'}{\partial x_2} \right)_{-A/2} \quad (13)$$

Reformulating Eq. (2) in terms of  $v'_1$  (i.e.  $v'_1 = v_1(x_2) - V_1$ ), substituting into Eq. (13), and integrating twice with respect to  $x_2$  between limits  $-A/2$  and  $x_2$  yields:

$$\begin{aligned} dc'(x_2) - d(C_w - C) &= V_1 \left( -\frac{A^2}{32} + \frac{x_2^2}{4} - \frac{x_2^4}{2A^2} \right) \frac{\partial C}{\partial x_1} \\ &+ d \left( \frac{\partial c'}{\partial x_2} \right)_{A/2} \left( \frac{x_2^2}{2A} + \frac{x_2}{2} + \frac{A}{8} \right) \\ &+ d \left( \frac{\partial c'}{\partial x_2} \right)_{-A/2} \left( -\frac{x_2^2}{2A} + \frac{x_2}{2} + \frac{3A}{8} \right) \end{aligned} \quad (14)$$

Evaluating this expression at the wall (i.e.  $x_2 = A/2$ ) and applying  $c'(A/2) = C_w - C$  demonstrates that:

$$\left. \frac{\partial c'}{\partial x_2} \right|_{-A/2} = - \left. \frac{\partial c'}{\partial x_2} \right|_{A/2} \quad (15)$$

which verifies that the concentration distribution is symmetric about the middle of the aperture. Inserting Eq. (15) into Eq. (14) gives:

$$\begin{aligned} c'(x_2) &= C_w - C + \frac{V_1}{d} \left( -\frac{A^2}{32} + \frac{x_2^2}{4} - \frac{x_2^4}{2A^2} \right) \frac{\partial C}{\partial x_1} \\ &+ \left( \frac{x_2^2}{A} - \frac{A}{4} \right) \left( \frac{\partial c'}{\partial x_2} \right)_{A/2} \end{aligned} \quad (16)$$

Integrating Eq. (16) with respect to  $x_2$  over the aperture width and rearranging yields:

$$\left. \frac{\partial c'}{\partial x_2} \right|_{A/2} = \frac{6}{A} (C_w - C) - \frac{V_1 A}{10d} \frac{\partial C}{\partial x_1} \quad (17)$$

Substituting Eq. (17) into Eq. (16) gives:

$$\begin{aligned} c'(x_2) &= (C_w - C) \left( -\frac{1}{2} + 6 \frac{x_2^2}{A^2} \right) \\ &+ \left( -\frac{A^2}{160} + \frac{3x_2^2}{20} - \frac{x_2^4}{2A^2} \right) \frac{V_1}{d} \frac{\partial C}{\partial x_1} \end{aligned} \quad (18)$$

Applying Eqs. (15) and (17) gives the wall concentration gradient:

$$\frac{d}{A} \left( \frac{\partial c'}{\partial x_2} \right)_{-A/2} = \frac{12d}{A^2} (C_w - C) - \frac{V_1}{5} \frac{\partial C}{\partial x_1} \quad (19)$$

multiplying both sides of Eq. (18) with  $v'_1$ , and averaging across the aperture gives the covariance term:

$$\overline{c'v'_1} = -(C_w - C) \frac{V_1}{5} - \frac{V_1^2 A^2}{700d} \frac{\partial C}{\partial x_1} \quad (20)$$

Now, we have models for the unknown terms in Eq. (10). By substituting Eq. (19) and the derivative of Eq. (20) into Eq. (10), the effective mean velocity, macroscopic dispersion coefficient, and upscaled first-order mass transfer coefficient, for the 1-D macroscopic transport equation, Eq. (6), are:

$$V_1^* = \frac{7}{5} V_1 \quad D^* = d + \frac{V_1^2 A^2}{700d} \quad K^* = \frac{12d}{A^2} \quad (21)$$

These macroscopic coefficients provide the means to predict the transport of a solute to flow between parallel plates with constant wall concentration. The upscaled mass transfer coefficient leads to a constant pore-scale Sherwood number [30]:

$$Sh^* = \frac{K^* A^2}{d} = 12 \quad (22)$$

#### 2.4. Model validation

To validate the macroscopic model, the 2D transport equation, Eq. (1), is solved numerically using an explicit finite difference scheme (a similar approach was originally reported by Schmidt and Zeldin [31]). Other numerical codes for solute transport are also available to solve this problem, e.g., [39]. In the finite difference scheme, spatial derivatives of concentration are approximated by central differences. Forward difference is used to approximate the temporal derivative, thus the equation at each grid point can be solved explicitly from the discrete concentration field at the previous time step. The number of grid points in the  $x_1$  and  $x_2$  directions are 400 and 200, respectively. The length of the domain was adjusted for each  $Pe$  to capture and resolve the entire developing region. The time step is based on a Courant-type estimate to insure stability of

the simulation. The simulation is run to steady state defined by the convergence to an asymptotic value of concentration at each grid point. Prior to the reported simulations, the numerical method was shown to be grid independent and was validated against the classic Taylor dispersion problem.

### 3. Results and discussion

In this section, the macroscopic model is evaluated for Peclet number in the range 0.01 to  $1 \times 10^4$ . A typical value for molecular diffusivity of cations, anions, and other solutes in water is  $0.001 \text{ mm}^2/\text{s}$ . Berkowitz and Zhou [4] report that for the rock fracture problem the aperture length is typically in the range of 0.01–1 mm, and the expected velocity range is 0.001–0.1 mm/s. Thus, for the rock fracture problem the Peclet number ranges from roughly 0.01–100, which is comparable for pore-scale problems [5]. We have extended the upper bound of the range of interest to  $1 \times 10^4$  for possible applications corresponding to large  $Pe$ , such as many heat transfer problems. For water with kinematic viscosity of  $1 \text{ mm}^2/\text{s}$  the corresponding Reynolds number range is  $1 \times 10^{-5}$ –10. Thus, we expect that the flow for this range of  $Pe$  is in the laminar flow regime.

The objective is to validate the macroscopic model by comparing to the numerical simulation. In addition, we will compare to the Graetz solution, which is well suited for large  $Pe$  in the steady regime.

#### 3.1. Mean concentration

Taking the steady state form of Eq. (6) and substituting a new variable  $C^* = C - C_w$  yields a second-order ordinary differential equation with respect to  $x_1$ :

$$D^* \frac{\partial^2 C^*}{\partial x_1^2} - V^* \frac{\partial C^*}{\partial x_1} - K^* C^* = 0 \tag{23}$$

The solution is

$$C^* = -C_w \exp(mx_1) \tag{24}$$

where

$$m = \frac{V^*}{2D^*} - \frac{1}{2} \sqrt{\left(\frac{V_1^*}{D^*}\right)^2 + 4\frac{K^*}{D^*}} \tag{25}$$

Fig. 2 shows the comparisons between the analytical, Graetz, and numerical profiles. For the numerical simulation profiles, the concentration values at the 200 grid points in the  $x_2$  direction are combined to yield the plotted average value, and every fourth grid point in the  $x_1$  direction is shown. The mean concentration is zero at the inlet and increases as dissolution from the wall occurs. Once the mean concentration reaches the wall concentration, the concentration distribution between the plates is uniform and mass transfer ceases. This implies that both the covariance and the wall concentration gradient approach zero, which is discussed below. For  $Pe = 0.01$  and 1 the macroscopic model shows good agreement with the numerical

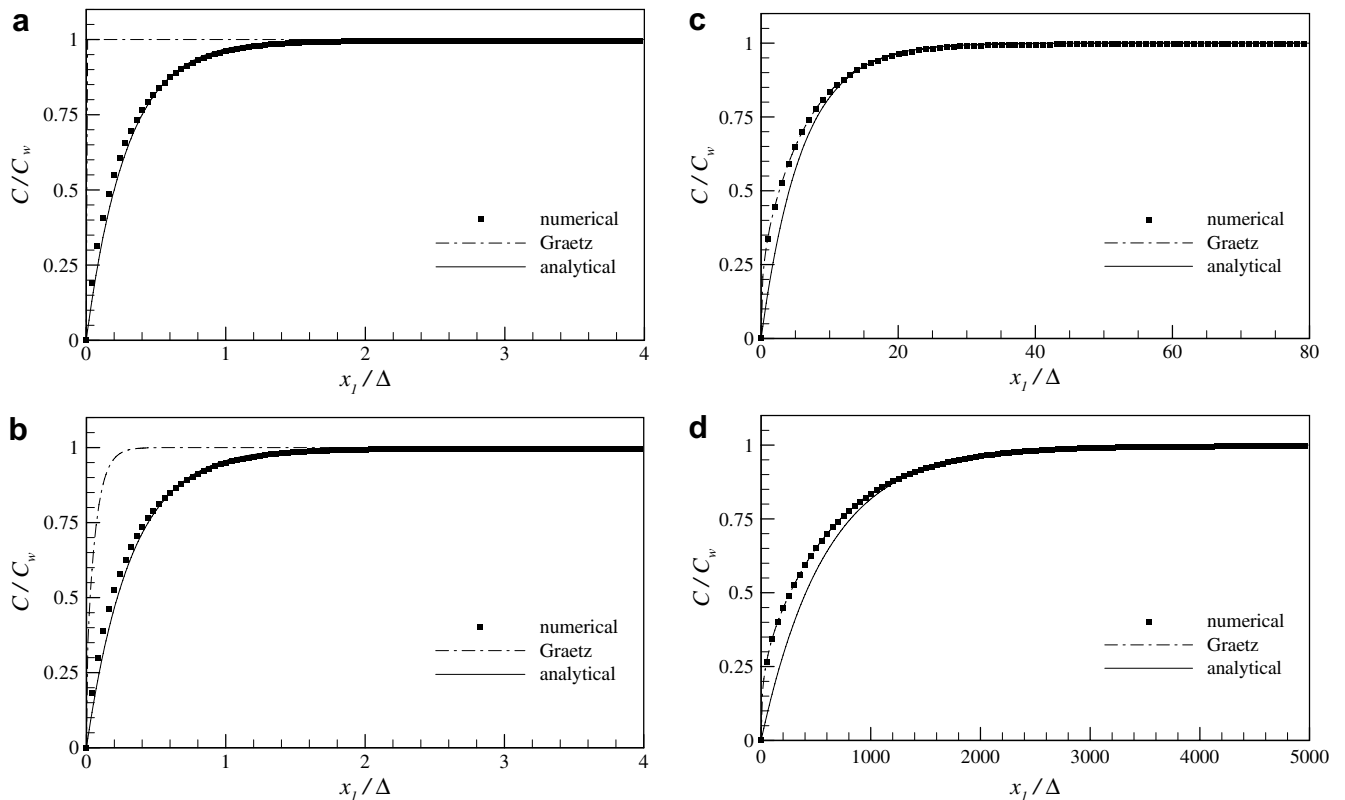


Fig. 2. Mean concentration for (a)  $Pe = 0.01$ , (b)  $Pe = 1$ , (c)  $Pe = 100$ , (d)  $Pe = 1 \times 10^4$ .

profile, although it appears to slightly underpredict the mean concentration for  $x_1/\Delta$  less than 0.5. As expected, the Graetz solution performs poorly in this range of  $Pe$  because longitudinal diffusion effects have been ignored.

For  $Pe = 100$  the domain length is much longer due to the increased velocity (and hence advection) in the  $x_1$  direction. The Graetz solution agrees with the numerical profile very well, whereas the macroscopic transport model solution again slightly underpredicts the mean concentration near the inlet ( $x_1/\Delta < 15$ ). For the  $Pe = 1 \times 10^4$  case, the Graetz solution agrees very well with the numerical profile which confirms its validity in this range. Overall, the macroscopic transport model gives a good approximation of the mean concentration profile, especially for  $Pe$  less than 100.

The difference between the analytical and numerical profiles near the inlet results from the assumption between Eqs. (12) and (13) that  $\partial c'/\partial x_1 \approx 0$ . In the current geometry, a high concentration gradient exists at the walls as the dissolution process starts near the inlet. The concentration profile changes rapidly as mass is transported transversely, hence the variation of  $c'$  with respect to  $x_1$  is not small in this region. Therefore, the elimination of the  $V_1 \frac{\partial c'}{\partial x_1}$  term in Eq. (13) leads to the underprediction of  $C$  in Fig. 2. Nevertheless, the macroscopic analytical model approaches the numerical solution a short distance downstream of the inlet, which indicates that the model is robust downstream. In fact, the macroscopic analytical model correctly predicts the distance downstream that the concentration equals, for example,  $0.85C_w$  for each  $Pe$ , which covers a range of six orders of magnitude.

### 3.2. Covariance and wall concentration gradient

The covariance of Eq. (20) is a good measure of the model validity because it depends on both the mean velocity and dispersion coefficient. Fig. 3 shows the comparison between the analytical and numerical profiles. Only the  $Pe = 1$  case is shown here because the profiles are similar for the other cases. The analytical model agrees well with the numerical simulation downstream from the inlet. The

covariance approaches zero because at large distances from the inlet, the concentration variation,  $c'$ , goes to zero as the concentration becomes uniform. The covariance is negative because the concentration and velocity deviations are negatively correlated. For instance, near the centerline the concentration is less than the mean ( $c' < 0$ ), whereas the velocity is greater than the mean ( $v'_1 > 0$ ). The reverse situation is present near the walls, therefore  $\overline{c'v'_1} < 0$ .

Near the inlet, the numerical solution increases from zero, reaches a local maximum value then decreases toward zero. The covariance is zero at the inlet because the cross-stream profile is uniformly zero, hence  $c'$  is zero. The analytical macroscopic model deviates from the numerical solution and fails to capture the change in slope of the profile because the macroscopic model assumes that  $\partial c'/\partial x_1 \approx 0$  as discussed above.

Eq. (19) gives the analytical expression for the concentration gradient in the transverse direction evaluated at the walls. This quantity is also a good measure of the model validity because it depends on both the mean velocity and dissolution rate coefficient. Fig. 4 shows the comparison between the analytical and numerical solutions. Again, only the  $Pe = 1$  case is shown because each case is similar. The profile decreases to zero because the concentration becomes uniform at large  $x_1$ . As with the previous results, the agreement with the numerical solution is good for large  $x_1$ , but the profiles show poorer agreement near the inlet. The steep slope of the profile near the inlet in Fig. 4, in fact, confirms that the  $\partial c'/\partial x_1 \approx 0$  assumption is not particularly good in this region.

### 3.3. Time evolution

Eq. (6) also predicts the time evolution of the mean concentration (in this section Eq. (6) was numerically integrated with respect to time). Note that the Graetz solution is only relevant for the steady state case, therefore comparison in this section is limited to the numerical simulation of the 2D transport equation. Fig. 5 shows the time record of mean concentration at three locations for the  $Pe = 1$  case. The macroscopic model shows good agreement for large

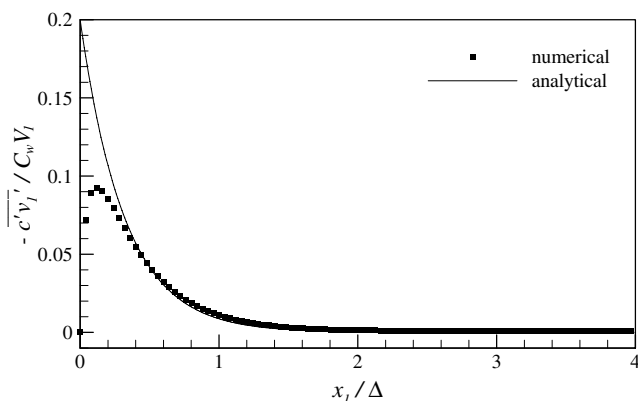


Fig. 3. Covariance for  $Pe = 1$ .

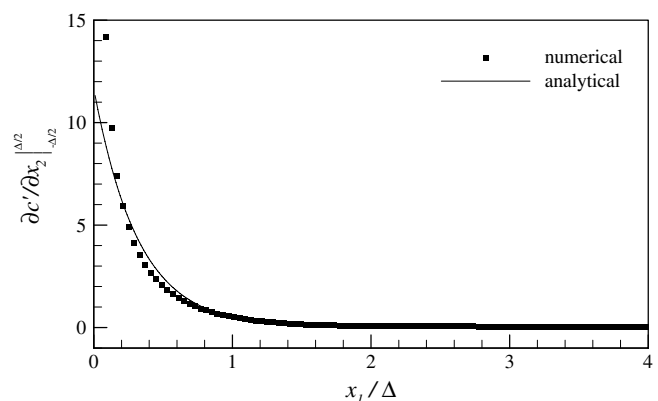


Fig. 4. Wall concentration gradient for  $Pe = 1$ .

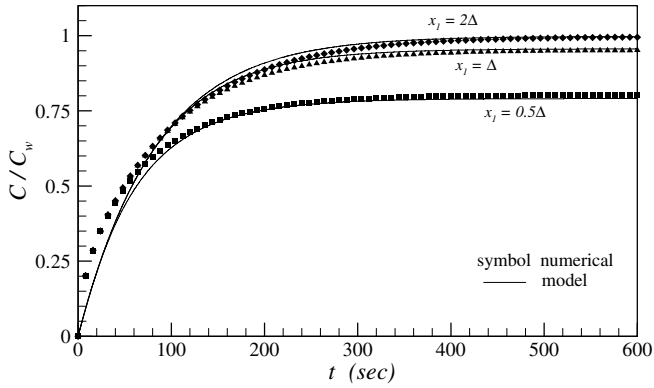


Fig. 5. Time records for  $Pe = 1$ .

time, but appears to underpredict the numerical solution at the start of the calculation ( $t < 80$  s). The original Taylor [35] analysis suffers from a similar limitation because it assumes that  $\partial c' / \partial x_2$  is small. This condition is violated immediately after the flow is started; Fischer et al. [13] report that time must be greater than  $0.4A^2/d$  for the assumption, and hence the model, to hold.

### 3.4. Effective macroscopic transport coefficients

It is interesting to note that the upscaled transport parameters in Eq. (21) show different characteristics from previous analyses. In the presence of the constant wall concentration, the effective mean velocity increases from  $V_1$  to  $\frac{7}{5}V_1$ , partially resulting from the diffusive mass flux from the wall, which is controlled by the concentration gradient at the walls, Eq. (19), and partially due to the covariance between the concentration and velocity perturbation fields, Eq. (20), which typically only causes macrodispersion.

The asymptotic macrodispersion coefficient,  $D^*$ , consists of two terms: one is the molecular diffusion coefficient, whereas the other is proportional to  $Pe^2$ , i.e.  $D^* = d + \frac{Pe^2 d}{2800}$ . In addition, the macrodispersion coefficient derived here is smaller than the well-known result for Taylor–Aris dispersion, given by  $D^* = d + \frac{V_1^2 A^2}{210d} = d + \frac{Pe^2 d}{840}$ , indicating that the mass transfer from the walls decreases the concentration variation, and that longitudinal diffusion needs to be considered in a larger range of  $Pe$ .

Furthermore, although the mass flux from the wall to the fluid is a function of longitudinal position, the upscaled first-order mass transfer coefficient,  $K^*$  depends only on the aperture and diffusion coefficient and is independent of the travel distance along  $x_1$  and velocity. If the customary method, i.e. directly equating the diffusive flux from the walls to first-order mass transfer, is applied to approximate the first-order mass transfer coefficient, one can obtain:

$$K_x^e = K^* - \frac{V_1}{5(C_w - C)} \frac{\partial C}{\partial x_1} \quad (26)$$

and

$$Sh_x^e = Sh^* - \frac{V_1 A^2}{5d(C_w - C)} \frac{\partial C}{\partial x_1} \quad (27)$$

where  $K_x^e$  and  $Sh_x^e$  are the effective first-order mass transfer coefficient and effective Sherwood number, respectively, determined by the diffusive mass flux. Because  $\frac{\partial C}{\partial x_1} \geq 0$  at steady state,  $K^* \geq K_x^e$  and  $Sh^* \geq Sh_x^e$ . In other words, the mass flux predicted by the upscaled macroscopic first-order mass transfer model in Section 2 is greater than the diffusive mass flux. Substituting the steady state solution, Eq. (24), for small  $Pe$ , into Eq. (27) yields:

$$Sh_x^e = 12 + \frac{Pe}{10} m \Delta \quad (28)$$

which is also independent of the spatial coordinate, but is a function of  $Pe$ . Note that  $m$  is negative, indicating the effective Sherwood number determined by the diffusive mass flux is smaller than 12. For  $Pe \gg 1$ , Eq. (28) can be approximated by (see Appendix),

$$Sh_x^e = 10.3 \quad (29)$$

Fig. 6 shows the Sherwood number decreases with increasing  $Pe$ . The effective Sherwood number of Eq. (28), determined by the complete diffusive mass flux from the wall, is a function of  $Pe$  at small  $Pe$ , and approaches 10.3 at large  $Pe$ .

The Graetz solution of Eqs. (4) and (5) can also be employed to evaluate the diffusive mass flux from the wall and the effective Sherwood number for  $Pe > 100$ . Substituting Eq. (5) into (27) leads to

$$Sh_x^e = 12 - \frac{8}{15} \frac{\sum K_n Z_n \lambda_n^2 \exp(-\lambda_n^2 x_1')}{\sum K_n Z_n \exp(-\lambda_n^2 x_1')} \quad (30)$$

which is a function of distance from the inlet. For values of  $x_1' > 0.2$  the value of the effective Sherwood number of Eq. (30), calculated by the parameters listed in Table 1, approaches 10.5 for all  $Pe > 100$ . Hence, the estimate of the effective Sherwood number in this approach is also a constant, with a value slightly greater than the value estimated

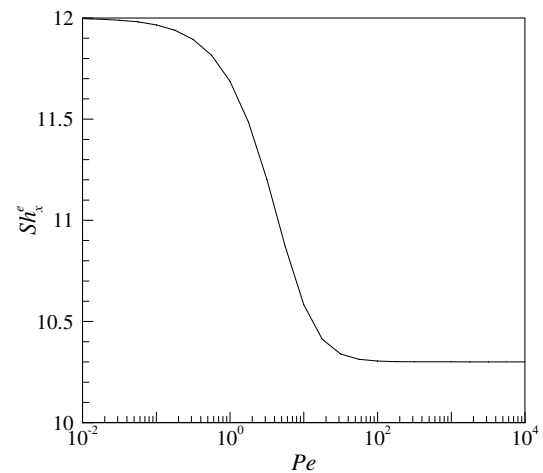


Fig. 6. The effective Sherwood number, Eq. (28), determined by the complete diffusive mass flux from the wall as a function of  $Pe$ . To generate the curve shown, the diffusion coefficient is assumed to be  $0.001 \text{ mm}^2/\text{s}$ , the plate gap is  $0.01 \text{ mm}$ , and  $Pe$  varies by adjusting  $V_1$ .

by the macroscopic analytical model discussed above, Eq. (29).

#### 4. Conclusions

A 1-D macroscopic transport model has been upscaled for initially clear fluid flowing between parallel plates with constant concentration. The transport problem in this idealized geometry may be solved numerically. For example, the finite difference and Graetz solutions are two solutions discussed in Section 2. However, our results provide coefficients of the effective mean velocity, macrodispersion coefficient, and upscaled first-order mass transfer rate (Eq. 21) for the mean transport equation (Eq. 6). The model is evaluated over a wide range of Peclet number (0.01 to  $1 \times 10^4$ ), which spans the diffusion- and advection-dominated transport regimes. The mean concentration profile predicted by the macroscopic model agrees well with a finite difference numerical simulation of the 2D transport equation, especially in the range of  $Pe \ll 100$ . The Graetz solution performs poorly in this regime, indicating that longitudinal diffusion cannot be neglected. Conversely for  $Pe \gg 100$  the Graetz solution agrees very well with the finite difference numerical solution. In this regime, the current upscaled model performs well downstream, but underpredicts the average concentration near the inlet.

The macroscopic model shows that the presence of the constant concentration boundaries and local-scale variations leads to the increase of the effective mean velocity and decrease of the macrodispersion coefficient compared to the Taylor–Aris dispersion. Further, the model yields a constant upscaled first-order mass transfer coefficient (the Sherwood number is 12). In our macroscopic model, the mass diffused from the walls of constant concentration is not directly used to approximate the first-order mass transfer coefficient because the diffusive mass flux is also characterized by the change of the first-order moment, i.e., the effective mean velocity. The effective Sherwood number determined by the complete diffusive mass flux is a function of the Peclet number at small Peclet number and approaches 10.3 at large Peclet number. In contrast, the effective Sherwood number evaluated by the Graetz solution is a function of the travel distance, and approaches 10.5 at large distance from the inlet.

The derived macroscopic model can be incorporated into more comprehensive modeling efforts. For instance, the model reported herein is more applicable than the Taylor shear dispersion solution for the model developed by Berkowitz and Zhou [4]. The analytical model can be applied to precipitation kinetics, which is the reverse of dissolution [24]. Furthermore, desorption of solutes from the walls could be modeled similarly, but the 2D transport equation would have to contain a retardation factor to account for sorption processes [37]. Non-equilibrium processes may also be employed to describe sorption/desorption [25]. In addition, the model and the methodology can be extended to a pore-network [2]. Bioremediation

and the dynamics between the change of the pore geometry and NAPL dissolution may also be included [8]. Evolution of the wall position and concentration due to dissolution would lead to more complex flows that would require solving the Navier–Stokes equations along the wall boundaries. Finally, the idealized geometry may be modified to include variable cross-sectional area [11], wall roughness [20], and composite porous-media lined channels [21].

#### Acknowledgements

Thanks to Dr. V. Kapoor for suggesting this project and Dr. K.D. Pennell for helpful discussion. This work was partially supported by a grant from the National Science Foundation (EAR-9803663).

#### Appendix

For  $Pe \gg 1$ , by neglecting the diffusion coefficient, the effective macroscopic dispersion coefficient can be simplified to

$$D^* = \frac{V_1^2 \Delta^2}{700d} = \frac{Pe^2 d}{2800} \quad (31)$$

Substituting Eqs. (21), (25), and (31) into (28) leads to

$$Sh_x^e = 12 + \frac{Pe}{20} \left( \frac{V^* \Delta}{D^*} \right) - \frac{Pe}{20} \sqrt{\left( \frac{V^* \Delta}{D^*} \right)^2 + 4 \left( \frac{K^* \Delta^2}{D^*} \right)} \quad (32)$$

$$Sh_x^e = 12 + \frac{Pe}{20} \frac{7}{5} \frac{2800}{Pe^2} \frac{V_1 \Delta}{d} - \frac{Pe}{20} \sqrt{\left( \frac{7}{5} \frac{2800}{Pe^2} \frac{V_1 \Delta}{d} \right)^2 + 4 \left( \frac{12 \cdot 2800}{Pe^2} \right)} \quad (33)$$

$$Sh_x^e = 10.3 \quad (34)$$

#### References

- [1] Agrawal HC. Heat transfer in laminar flow between parallel plates at small Peclet numbers. *Appl Sci Res A* 1960;9:177–89.
- [2] Ahmadi A, Aigueperse A, Quintard M. Upscaling of nonwetting phase residual transport in porous media: a network approach. *Transp Porous Media* 2001;43:309–53.
- [3] Aris R. On the dispersion of a solute in a fluid flowing through a tube. *Proc Roy Soc London A* 1956;235:67–77.
- [4] Berkowitz B, Zhou J. Reactive solute transport in a single fracture. *Water Resour Res* 1996;32:901–13.
- [5] Bijeljic B, Muggeridge AH, Blunt MJ. Pore-scale modeling of longitudinal dispersion. *Water Resour Res* 2004;40:W11501.
- [6] Brenner H, Edwards DA. *Macrotransport processes*. Boston: Butterworth-Heinemann; 1993.
- [7] Chrysikopoulos CV. Three-dimensional analytical models of contaminant transport from non-aqueous phase liquid pool dissolution in saturated subsurface formations. *Water Resour Res* 1995;31:1137–45.
- [8] Chu M, Kitanidis PK, McCarty PL. Effects of biomass accumulation on microbially enhanced dissolution of a PCE pool: a numerical simulation. *J Contam Hydrol* 2003;65:79–100.
- [9] Chu M, Kitanidis PK, McCarty PL. Dependence of lumped mass transfer coefficient on scale and reactions kinetics for biologically enhanced NAPL dissolution. *Adv Water Resour* 2007;30:1618–29.

- [10] Deavours CA. An exact solution for the temperature distribution in parallel plate Poiseuille flow. *J Heat Transfer* 1974;96:489–95.
- [11] Detwiler RL, Rajaram H, Glass RJ. Solute transport in variable-aperture fractures: an investigation of the relative importance of Taylor dispersion and macrodispersion. *Water Resour Res* 2000;36:1611–25.
- [12] EPA. A guide to principal threat and low level threat wastes. Publication 9380.3-06FS. Washington, DC: EPA Office of Solid Waste and Emergency Response, 1991.
- [13] Fischer HB, List EJ, Koh RCY, Imberger J, Brooks NH. Mixing in inland and coastal waters. San Diego, CA: Academic Press; 1979.
- [14] Gramling CM, Harvey CF, Meigs LC. Reactive transport in porous media: a comparison of model prediction with laboratory visualization. *Environ Sci Technol* 2002;36:2508–14.
- [15] Hölttä P, Hakanen M, Hautajärvi A, Timonen J, Väättäinen K. The effects of matrix diffusion on radionuclide migration in rock column experiments. *J Contamin Hydrol* 1996;21:165–73.
- [16] Hull LC, Miller JD, Clemo TM. Laboratory and simulation studies of solute transport in fracture networks. *Water Resour Res* 1987;23:1505–13.
- [17] Imhoff PT, Jaffe PR, Pinder GF. An experimental study of complete dissolution of a nonaqueous phase liquid in saturated porous media. *Water Resour Res* 1994;30:307–20.
- [18] Kapoor V, Gelhar LW, Miralles-Wilhelm F. Bimolecular second-order reactions in spatially varying flows: segregation induced scale-dependent transformation rates. *Water Resour Res* 1997;33:527–36.
- [19] Kays WM, Crawford ME. Convective heat and mass transfer. 2nd ed. New York: McGraw-Hill; 1980.
- [20] Koplik J, Ippolito I, Hulin JP. Tracer dispersion in rough channels: a two-dimensional numerical study. *Phys Fluids A* 1993;5:1333–43.
- [21] Kuznetsov AV. Influence of thermal dispersion on forced convection in a composite parallel-plate channel. *Z Angew Math Phys* 2001;52:135–50.
- [22] Lee KY, Chrysikopoulos CV. NAPL pool dissolution in stratified and anisotropic porous formations. *J Environ Eng* 1998;124:851–62.
- [23] Miller CT, Poirier-McNeill MM, Mayer AS. Dissolution of trapped nonaqueous phase liquids: mass transfer characteristics. *Water Resour Res* 1990;26:2783–96.
- [24] Morel FMM. Principles of aquatic chemistry. New York: John Wiley and Sons; 1983.
- [25] Neville CJ, Ibaraki M, Sudicky EA. Solute transport with multiprocess nonequilibrium: a semi-analytical solution approach. *J Contamin Hydrol*. 2000;44:141–59.
- [26] Nusselt W. Der Wärmeaustausch am Berieselungskühler. *Z Vereines Deut Ing* 1923;67:206–10.
- [27] Parsons AM, Olague NE, Gallegos DP. Conceptualization of a high-level nuclear waste repository site in unsaturated, fractured tuff. US Nuclear Regulatory Commission NUREG/CR-5495, 1991.
- [28] Powers SE, Abriola LM, Weber Jr WJ. An experimental investigation of nonaqueous phase liquid dissolution in saturated subsurface systems: steady state mass transfer rates. *Water Resour Res* 1992;28:2691–705.
- [29] Raje DS, Kapoor V. Experimental study of bimolecular reaction kinetics in porous media. *Environ Sci Technol* 2000;34:1234–9.
- [30] Sahloul NA, Ioannidis MA, Chatzis I. Dissolution of residual non-aqueous phase liquids in porous media: pore-scale mechanisms and mass transfer rates. *Adv Water Resour* 2002;25:33–49.
- [31] Schmidt FW, Zeldin B. Laminar heat transfer in the entrance region of ducts. *Appl Sci Res* 1970;23:73–94.
- [32] Seagren EA, Rittmann BE, Valocchi AJ. Quantitative-evaluation of the enhancement of NAPL-pool dissolution by flushing and biodegradation. *Environ Sci Technol* 1994;28:833–9.
- [33] Sellars JR, Tribus M, Klein JS. Heat transfer to laminar flow in a round tube or flat conduit – the Graetz problem extended. *Trans ASME* 1956;78:441–8.
- [34] Shah RK, London AL. Laminar flow forced convection in ducts: a source book for compact heat exchanger analytical data. New York: Academic Press; 1978.
- [35] Taylor G. Dispersion of soluble matter in solvent flowing slowly through a tube. *Proc Roy Soc London A* 1953;219:186–203.
- [36] Weigand B. An exact analytical solution for the extended turbulent Graetz problem with Dirichlet wall boundary conditions for pipe and channel flows. *Int J Heat Mass Transfer* 1996;39:1625–37.
- [37] Wels C, Smith L, Beckie R. The influence of surface sorption on dispersion in parallel plate fractures. *J Contamin Hydrol* 1997;28:95–114.
- [38] Wylie CR, Barrett LC. Advanced engineering mathematics. 5th ed. New York: McGraw-Hill; 1982.
- [39] Zheng C, Wang PP. MT3DMS, A modular three-dimensional multi-species transport model for simulation of advection, dispersion and chemical reactions of contaminants in groundwater systems: documentation and user guide. US Army Engineer Research and Development Center Contract Report SERDP-99-1, Vicksburg, MS, 1999.